Transition from order to chaos in reduced quantum dynamics

Waldemar Kłobus [1], Paweł Kurzyński [2], Marek Kuś [3], Wiesław Laskowski [1,4]
Robert Przybycień [3] and Karol Życzkowski [5,3]
[1] Institute of Theoretical Physics and Astrophysics, Faculty of Mathematics, Physics and Informatics, University of Gdańsk, 80-308 Gdańsk, Poland
[2] Institute of Spintronics and Quantum Information, Faculty of Physics, Adam Mickiewicz University, 61-614 Poznań, Poland
[3] Center for Theoretical Physics, Polish Academy of Sciences, Al. Lotników 32/46, 02-668 Warszawa, Poland
[4] International Centre for Theory of Quantum Technologies, University of Gdańsk, 80-308 Gdańsk, Poland
[5] Institute of Theoretical Physics, Jagiellonian University, Lojasiewicza 11, 30-348 Kraków, Poland

(Received 26 November 2021; accepted 15 February 2022; published 2 March 2022)

We study a damped kicked top dynamics of a large number of qubits ($N \to \infty$) and focus on an evolution of a reduced single-qubit subsystem. Each subsystem is subjected to the amplitude damping channel controlled by the damping constant $r \in [0, 1]$, which plays the role of the single control parameter. In the parameter range for which the classical dynamics is chaotic, while varying r we find the universal period-doubling behavior characteristic to one-dimensional maps: period-2 dynamics starts at $r_1 \approx 0.3181$, while the next bifurcation occurs at $r_2 \approx 0.5387$. In parallel with period-4 oscillations observed for $r \leqslant r_3 \approx 0.5672$, we identify a secondary bifurcation diagram around $r \approx 0.544$, responsible for a small-scale chaotic dynamics inside the attractor. The doubling of the principal bifurcation tree continues until $r \leqslant r_\infty \sim 0.578$, which marks the onset of the full scale chaos interrupted by the windows of the oscillatory dynamics corresponding to the Sharkovsky order. Finally, for $r = 1$ the model reduces to the standard undamped chaotic kicked top.

DOI: 10.1103/PhysRevE.105.034201

I. INTRODUCTION

Studies on classical nonlinear systems became of a great significance due to the numerous applications to physics, chemistry, biology, and engineering [1]. One of the key achievements of these early investigations consists in understanding of the route from regular to chaotic dynamics [2,3]. Furthermore, a link between chaotic dynamics, defined by exponential sensitivity to initial conditions, and emergence of fractal structures was established [4]. Discovery of the Feigenbaum universality of the period doubling scenario in one-dimensional systems led to insights concerning the nonlinear dynamics [5–7].

A lot of attention was paid to investigate properties of quantum analogs of classically regular and chaotic systems [8], as their investigations helped to reveal fine connections between classical and quantum mechanics [9]. Although the standard unitary quantum evolution is linear, so no exponential sensitivity to initial conditions can be detected by a state-vector overlap, there exist quantum phenomena which reflect the presence of classical chaos. The study of these properties, called *quantum chaology* [10] significantly improved our understanding of the classical limit of quantized chaotic systems, as numerous *signatures of quantum chaos* were identified [11,12] and explained with help of the theory of random matrices [13] and theory of periodic orbits [14].

Several studies of classically chaotic dynamics and the corresponding unitary quantum evolution, which takes place in a finite dimensional Hilbert space, where performed with a model of kicked top [15]. It describes a spin undergoing constant precession around a fixed magnetic field subjected to a periodic sequence of nonlinear kicks. The corresponding quantum system is described by a unitary evolution operator, of a fixed dimension, $d = 2j + 1$, where the quantum number j is set by the squared angular momentum operator J^2 and eigenvalue $j(j + 1)$. If the kicking strength parameter β is large enough the classical dynamics on a sphere becomes chaotic and the spectral properties of the unitary evolution operator U can be described by an appropriate ensemble of random unitary matrices [16]. An apparent contradiction between exponential divergence of neighboring trajectories of a chaotic classical dynamical system and the linear evolution of the corresponding quantum system can be explained by the fact that the limit time to infinity, necessary to define the Lyapunov exponent, and the limit $j \to \infty$, corresponding to the classical limit of quantum theory, $\hbar \to 0$, do not commute [12].

Investigations of quantized chaotic dynamics are relevant not only for quantum theory but have also applications in several branches of experimental physics [17]. In particular, the model of quantum kicked top, motivated by an experimental work of Waldner *et al.* [18], was later studied experimentally [19,20]. The latter reference concerns nuclear magnetic resonance experiments simulating the model of coupled kicked tops, earlier analyzed in [21–24].

A physical realization of any model quantum dynamics is subjected to dissipation and decoherence. Although the original model of the quantum kicked top is described by unitary time evolution [15], it was later generalized [12,25] to take into account also effects of dissipation and decoherence.

The model of quantum kicked tops was used to analyze properties of entanglement in coupled chaotic systems [26–29]. Although the dynamics of the entire bipartite system is unitary, the dynamics of the reduced state corresponding to a given subsystem is nonunitary. Under the assumption of a strong coupling between subsystems, classically chaotic dynamics of individual tops, and large dimension of the system, the partial traces of the composite system display statistical properties characteristic of random density matrices [30].

As the Heisenberg time evolution of an isolated quantum state is unitary and linear, $\rho \to U\rho U^\dagger$, some nonlinear effects may arise due to interaction with other subsystems. For instance, the quadratic term ρ^2 corresponds to quantum measurements performed on two copies of the same quantum state ρ [31]. Other models include nonlinear transformations, in which individual entries of the density matrix are squared [32] and measurement based nonlinear rotation of the Bloch sphere [33].

In this work we are going to analyze a system of N interacting qubits, described in the Hilbert space of a finite dimension $d = 2^N$. Dynamics of a single qubit represents kicked top in the chaotic regime (kicking strength $\beta = 6$), and all the subsystems are coupled by an interaction Hamiltonian. Therefore, the reduced dynamics of a qubit subsystem becomes effectively nonlinear as $N \to \infty$.

The aim of this contribution is to analyze properties of the nonlinear dynamics of a single qubit, obtained by partial trace over remaining subsystems, under a realistic assumption that each subsystem is subjected to the amplitude damping channel. We demonstrate that depending on the value of the damping parameter r, equal for all subsystems, the dynamics of the reduced state exhibits various forms of very complex behaviors. In particular, we show under what conditions the single qubit dynamics converges to a stable fixed point and when bifurcation occurs. Furthermore, we demonstrate that the period doubling scenario, originally observed for classical systems [5,6], can be also applied to reduced dynamics of a damped quantum system. In such a way the Feigenbaum route to chaos can be now identified also for quantum systems. Apart from the standard period doubling scenario, inside the period-2 and period-4 oscillatory dynamics, we observe a self-similar structure of higher order bifurcation diagrams, responsible for a small-scale chaos inside the attractor. Similar structures were observed for the classical, two-dimensional Hénon map [34].

A complementary goal of this project concerns investigation of the purely quantum regime of the model obtained for a finite number of qubits. As fractal structures characteristic to classical chaotic dynamics become blurred by quantum effects [35–37], it is particularly interesting to observe how the fine effects related to the classical period doubling scenario and strange attractors get dominated by quantum effects. Let us emphasize here that the model of damped coupled kicked tops, investigated in this work, can be related to the physics of many body systems and interacting cold atoms.

This work is organized as follows. In Sec. II we introduce the model of damped coupled kicked tops and present some of its properties. Fixed points of the system describing the dynamics of single qubit, under the assumption of a large total number N of qubits, is presented in Sec. III. In Sec. IV we fix two parameters of the unitary evolution, so the system is solely described by the parameter r governing the amplitude damping, as $1 - r$ can be interpreted as the damping strength. The fixed parameters are chosen in such a way that in the unitary limit, $r \to 1$, the system becomes equivalent to the standard chaotic kicked top [15]. The period doubling scenario for such a nonlinear quantum system is analyzed in Sec. V while strange attractors are investigated in Sec. VI. In Sec. VII we study bifurcation diagrams and identify the windows of periodicity and in Sec. VIII we study Lyapunov exponents. Concluding remarks are presented in Sec. IX, while the derivation of the effective single-qubit dynamics in the limiting case $N \to \infty$ is provided in the Appendix.

II. MODEL QUANTUM SYSTEM

We consider a collection of N interacting qubits. Each qubit is a two-state quantum system. One can think of N interacting spins 1/2, however a particular physical implementation of the model is irrelevant for our discussion. The qubits are initially in a symmetric product state $\rho_0^{\otimes N}$ and we assume the following interaction Hamiltonian:

$$H = \frac{g}{2(N-1)}\left(\sum_{n=1}^{N}\sigma_z^{(n)}\right)^2, \tag{1}$$

where $\sigma_z^{(n)}$ is the Pauli-Z operator acting on the nth qubit and g determines the interaction strength. If $g = \mathcal{O}(1)$ and $N \to \infty$, then each qubit from this collection undergoes an effective nonlinear unitary dynamics $U(\rho)\rho U^\dagger(\rho)$ (see the Appendix), where

$$U(\rho) = e^{-i(\beta/2)\langle\sigma_z\rangle\sigma_z}, \tag{2}$$

$\langle\sigma_z\rangle = \mathrm{Tr}\{\rho\sigma_z\}$, $\beta = g\tau$, and τ is the time of interaction.

Next, we modify the evolution analyzed. The map is going to consist of three subsequent operations: (1) the above nonlinear unitary evolution $U(\rho)$, (2) local rotation of each qubit about the y axis, and (3) amplitude damping to $|0\rangle$ state. The operations (1) and (2) generate the standard kicked top dynamics [15,16] described by

$$V(\rho) = e^{-i\frac{\alpha}{2}\sigma_y}U(\rho), \tag{3}$$

where α is the angle of rotation about the y axis. The total evolution is given by

$$\rho_{t+1} = K_1V(\rho)\rho_tV^\dagger(\rho)K_1^\dagger + K_2V(\rho)\rho_tV^\dagger(\rho)K_2^\dagger. \tag{4}$$

In the above,

$$K_1 = \begin{pmatrix}1 & 0\\ 0 & \sqrt{r}\end{pmatrix},\quad K_2 = \begin{pmatrix}0 & \sqrt{1-r}\\ 0 & 0\end{pmatrix} \tag{5}$$

are the amplitude damping Kraus operators [38], which satisfy the desired identity resolution, $\sum_{i=1}^{2}K_i^\dagger K_i = \mathbb{I}$, equivalent to the trace preserving condition. The parameter $r \in [0, 1]$ describes the degree of damping in the model: for $r = 1$ the operator K_2 vanishes, so $r' = 1 - r$ plays the role of the damping strength.

After t steps the state of the qubit is given by

$$\rho_t = \tfrac{1}{2}(\mathbb{1} + x_t\sigma_x + y_t\sigma_y + z_t\sigma_z), \tag{6}$$

where $\mathbf{v}_t = (x_t, y_t, z_t)$ is the corresponding Bloch vector. The evolution of $\mathbf{v}_t$ is determined by

$$\begin{aligned} x_{t+1} &= \sqrt{r}\{[x_t\cos(\beta z_t) - y_t\sin(\beta z_t)]\cos\alpha + z_t\sin\alpha\},\\ y_{t+1} &= \sqrt{r}[x_t\sin(\beta z_t) + y_t\cos(\beta z_t)],\\ z_{t+1} &= 1 + r\{[y_t\sin(\beta z_t) - x_t\cos(\beta z_t)]\sin\alpha + z_t\cos\alpha - 1\}. \end{aligned} \tag{7}$$

III. FIXED POINTS AND BIFURCATIONS

Let $\mathbf{v}^* = (x^*, y^*, z^*)$ denote a fixed point of the evolution (7). It follows that

$$\begin{aligned} x^* &= \frac{\sqrt{r}\sin\alpha[1-\sqrt{r}\cos(\beta z^*)]z^*}{1 + r\cos\alpha - \sqrt{r}(\cos\alpha + 1)\cos(\beta z^*)},\\ y^* &= \frac{r\sin\alpha\sin(\beta z^*)z^*}{1 + r\cos\alpha - \sqrt{r}(\cos\alpha + 1)\cos(\beta z^*)},\\ z^* &= 1 + rz^*\cos(\alpha) - r + rz^*\sin^2(\alpha)\\ &\quad\times\frac{r-\sqrt{r}\cos(\beta z^*)}{1 + r\cos(\alpha) - \sqrt{r}[\cos(\alpha)+1]\cos(\beta z^*)}. \end{aligned} \tag{8}$$

This set of equations is not easy to solve, so we analyze them numerically. We define

$$\begin{aligned} f(z^*, r, \alpha, \beta) &= -z^* + 1 + rz^*\cos(\alpha) - r + rz^*\sin^2(\alpha)\\ &\quad\times\frac{r-\sqrt{r}\cos(\beta z^*)}{1 + r\cos(\alpha) - \sqrt{r}[\cos(\alpha)+1)\cos(\beta z^*]}, \end{aligned} \tag{9}$$

and the goal is to look for solutions to $f(z^*, r, \alpha, \beta) = 0$.

The next goal is to investigate the stability of these fixed points. To do this, we use the standard approach [1], i.e., we linearize the equations in a vicinity of a fixed point. More precisely, consider a small deviation from a fixed point,

$$\mathbf{v}_t = \mathbf{v}^* + \mathbf{\Delta v}_t. \tag{10}$$

It follows that

$$\mathbf{\Delta v}_{t+1} \approx \mathbf{A}_{\mathbf{v}^*}\mathbf{\Delta v}_t, \tag{11}$$

where $\mathbf{A}_{\mathbf{v}^*}$ is the Jacobian of the map at point $\mathbf{v}^*$. A fixed point $\mathbf{v}^*$ is stable if the modulus of all the eigenvalues of $\mathbf{A}_{\mathbf{v}^*}$ is not greater than 1.

IV. STABILITY OF THE MODEL

From now on we fix the parameters of the model,

$$\alpha = \frac{\pi}{2}, \quad \beta = 6, \tag{12}$$

as this choice leads to chaotic dynamics of the undamped kicked top in the classical limit [15]. Therefore, the system is now described solely by the unitarity parameter r. Its behavior in the two limiting cases is clear. For $r = 0$ the system undergoes damping to $|0\rangle$ in one step, whereas for $r = 1$ there is no damping in the system; the evolution becomes unitary and reduces to the chaotic dynamics of the standard kicked top. These two extreme values correspond to two different behaviors—order and chaos. Interesting things should happen in between and this is what we are going to examine below.

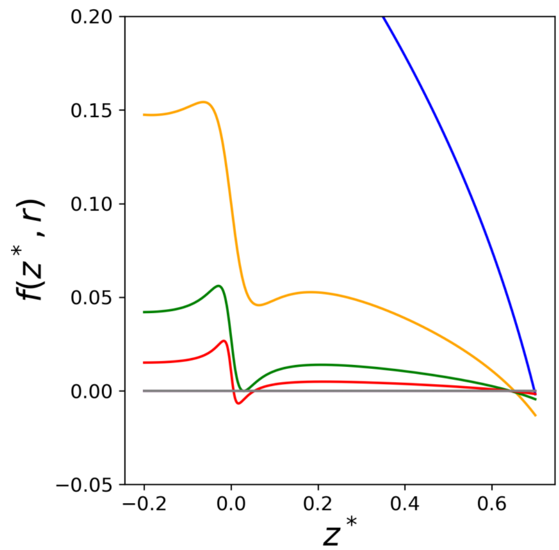

FIG. 1. The plot of $f(z^*, r)$ for: $r = 0.6$ (blue), $r = 0.9$ (orange), $r = 0.972 \approx r_b$ (green), $r = 0.99$ (red)

First, let us look for fixed points using $f(z^*, r) = f(z^*, r, \pi/2, 6)$—see Eq. (9). We find that for $0 \leqslant r < r_b \approx 0.9719$ there is one fixed point, denoted by $\mathbf{v}_0^*$. For $r_b < r < 1$ there are three of them: $\mathbf{v}_0^*$, $\mathbf{v}_1^*$, and $\mathbf{v}_2^*$. The additional two appear in a saddle-node bifurcation. Finally, for $r = 1$ there are two fixed points: $\mathbf{v}_0^*$ and $\mathbf{v}_2^*$. The fixed point $\mathbf{v}_1^*$ disappears due to discontinuity of $f(z^*, 1)$ at $z^* = 0$—see Fig. 1.

Through the analysis of the corresponding Jacobian

$$\mathbf{A}_{\mathbf{v}^*} = \begin{pmatrix} 0 & 0 & -\sqrt{r}\\ -\sqrt{r}s(z^*) & \sqrt{r}c(z^*) & -\beta\sqrt{r}[y^*s(z^*) + x^*c(z^*)]\\ rc(z^*) & rs(z^*) & \beta r[y^*c(z^*) - x^*s(z^*)] \end{pmatrix}, \tag{13}$$

where

$$s(z^*) \equiv \sin(\beta z^*), \quad c(z^*) \equiv \cos(\beta z^*), \tag{14}$$

with $\beta = 6$, we find that for $r \leqslant r_1 \approx 0.3181$ the single fixed point $\mathbf{v}_0^*$ is stable, whereas for $r > r_1$ it becomes unstable as a result of a flip bifurcation [1]. On the other hand, for $r > r_b$ the new fixed point $\mathbf{v}_1^*$ is stable and $\mathbf{v}_2^*$ is unstable. In addition, for $r = 1$ the fixed point $\mathbf{v}_0^*$ is unstable and the stability of $\mathbf{v}_2^*$ cannot be determined due to the fact that all eigenvalues of $\mathbf{A}_{\mathbf{v}_2^*}$ are equal to 1. However, since the value $r = 1$ corresponds to the standard kicked top, we know that $\mathbf{v}_2^*$ cannot be stable. Finally, the value of z_0^* equals 1 for $r = 0$ and monotonically decreases to ≈0.639 for $r = 1$, whereas the values of z_1^* and z_2^* are close to zero ($z_1^* < z_2^* < 0.06$).

V. PERIOD DOUBLING AND UNIVERSALITY

For $r_1 < r < r_b$ there are no stable fixed points. At $r = r_1$ we observe the onset of period-2 oscillations, i.e., after a transient stage the state-space of the system becomes limited to just two points and the evolution flips one point to the

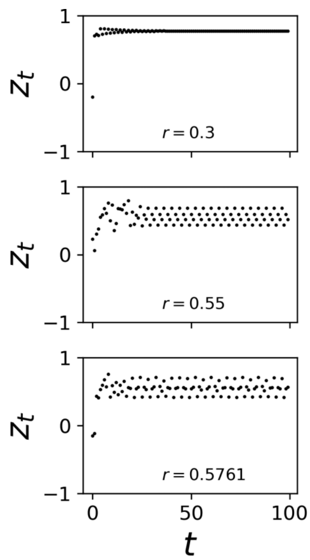

FIG. 2. The first 100 steps of the evolution of z_t for different values of r and a random initial state.

other. As r increases, the period of oscillations doubles. Interestingly, for $r_{s_1} \approx 0.5378 < r < r_{s_2} \approx 0.5455$ we observe a departure from the standard period-doubling behavior and emergence of higher-order bifurcation trees, which leads to a weakly chaotic dynamics inside the attractor. A self-similar structure is discussed in more details in Sec. VIII.

Examples of the evolution of z_t for six different values of r are presented in Fig. 2. The dependence of the asymptotic behavior on the parameter r is summarized in Table I. The value of r_∞, at which the onset of chaos occurs, is hard to determine in numerical experiments, since it is not easy to distinguish between multiperiod oscillations and the irregular chaotic dynamics. However, we are going to upper bound it in a moment.

The phenomenon of period doubling was first observed in the logistic map [5,6], but later it was found to occur in a large family of iterated maps that are described by a single parameter r—see [3,7]. For all these maps one can define a value r_k that marks the onset of period-2^k oscillations. Interestingly, Feigenbaum found a universal scaling behavior, namely that

TABLE I. Asymptotic behavior of the model for different values of r.

Range of r	Behavior
$0 \leqslant r < r_1 \approx 0.3181$	stationary
$r_1 < r < r_2 \approx 0.5387$	period 2
$r_{s_1} \approx 0.5378 < r < r_{s_2} \approx 0.5455$	self-similarity
$r_2 < r < r_3 \approx 0.5672$	period 4
$r_3 < r < r_4 \approx 0.5729$	period 8
$r_4 < r < r_5 \approx 0.5741$	period 16
...	...
$r_\infty < r < r_b \approx 0.9719$	chaos
$r_b < r < 1$	stationary
$r = 1$	chaos (kicked top)

TABLE II. Estimation of the ratio $(r_n - r_{n-1})/(r_{n+1} - r_n)$.

Ratio	Value
$(r_2 - r_1)/(r_3 - r_2)$	$\approx$7.74
$(r_3 - r_2)/(r_4 - r_3)$	$\approx$5.0
$(r_4 - r_3)/(r_5 - r_4)$	$\approx$4.75

the ratio $\frac{r_n - r_{n-1}}{r_{n+1} - r_n}$ tends to a constant value as n goes to infinity

$$\lim_{n\to\infty} \frac{r_n - r_{n-1}}{r_{n+1} - r_n} = \delta = 4.669\,201\,609\ldots. \quad (15)$$

The number δ is now known as the *Feigenbaum constant*.

The universal period-doubling behavior and the approximate convergence to the Feigenbaum constant was observed in a number of one-dimensional physical systems and mathematical models [5,6]. Below we demonstrate how an approximate convergence occurs in the three dimensional model analyzed in Table II.

The exact convergence to δ cannot be observed due to finite precision of numerical simulations. We estimated the values of the parameters r_k for $k = 1\ldots5$ up to the order 10^{-4}. Assuming that

$$\frac{r_5 - r_4}{r_6 - r_5} \approx \delta, \quad (16)$$

we can estimate $r_6 \approx 0.5743$. Since $r_{k+1} - r_k$ is rapidly decreasing, it is natural to conjecture that the value of r_∞ is close to r_6. Indeed, numerical simulations estimate that $r_\infty < 0.578$.

At first glance the bifurcation diagram presented in Fig. 3 is similar to the one of a logistics map and of other systems that exhibit period-doubling behavior [2,3,5]. It also shows yet another universal property of such systems—the emergence of windows of periodicity, i.e., the existence of regions in which the chaotic behavior ceases and periodic behavior re-emerges for some narrow regions of r. We find two transparent such windows in our system. The first one (narrow with five and ten

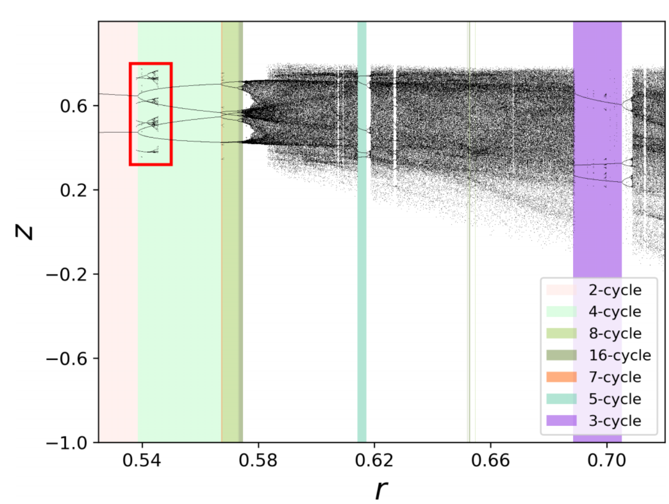

FIG. 3. Bifurcation diagrams for the Z coordinate of the Bloch vector with cycles identified according to the Sharkovsky order. Note secondary bifurcation diagrams located inside the four-cycle around $r \approx 0.545$ and magnified in Fig. 7.

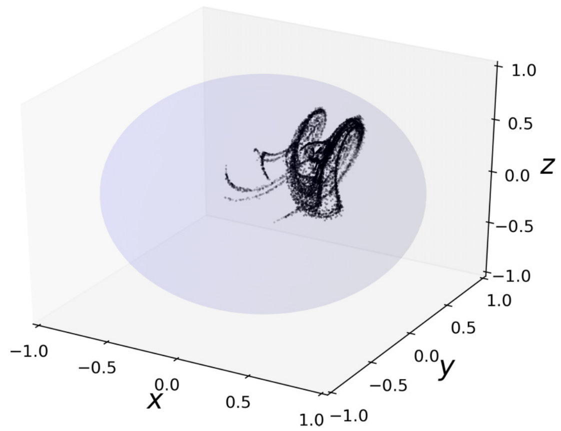

FIG. 4. Visualization of a strange attractor: 10 000 steps of a trajectory stemming from a random initial state dynamics for $r = 0.75$. Black points denote subsequent positions of the Bloch vector.

cycles) appears at the range $0.614 \leqslant r \leqslant 0.619$ and the second one (wider with three and six cycles) appears at the range $0.689 \leqslant r \leqslant 0.709$. This is in agreement with the celebrated Sharkovsky ordering, $1 \prec 2 \prec 4 \prec 8 \prec \cdots \prec 7 \prec 5 \prec 3$; see [39–41].

VI. CHAOS AND STRANGE ATTRACTOR

The onset of chaos occurs at $r = r_\infty$. Interestingly, for $r_b < r < 1$ the system returns to its stationary behavior. This is due to a saddle-node bifurcation that gives rise to a stable fixed point $\mathbf{v}_1^*$. Except for two narrow regions (see next sections), for $r_\infty < r < r_b$ the asymptotic dynamics of the Bloch vector takes place on an attractor that is a peculiar subset of a Bloch sphere—see Fig. 4. This is a strange attractor whose fractal dimension can be estimated with the help of *the correlation dimension* [42] in the following way. We initiate the system in a random state $\mathbf{v}_0$ and evolve it for 10 000 steps. Next, we randomly choose a point $\mathbf{w}$ on an attractor and define a ball of radius ε around it. We vary ε and count how many points generated by the evolution are inside this ball. We repeat this procedure for many different choices of $\mathbf{v}_0$ and $\mathbf{w}$. Finally, we calculate the average number of points $C(\varepsilon)$ inside the ball. This number should scale as [42]

$$C(\varepsilon) \propto \varepsilon^d, \tag{17}$$

where d is the correlation dimension of the attractor. Therefore, we plot $\ln C$ against $\ln \varepsilon$, which should be linear for some range of ε, and estimate the slope—see Fig. 5. We found that the correlation dimension of the strange attractor is less than 2. In particular, in the case $r = 0.75$ visualized in Fig. 4, its value reads $d \approx 1.84$.

VII. LYAPUNOV EXPONENTS AND BIFURCATION DIAGRAM

To describe the analyzed dynamics quantitatively we will use the standard notions of Lyapunov exponents and dynamical entropy. Given an initial Bloch vector $\mathbf{v}_0$ and an initial displacement $\delta\mathbf{v}_0 = \mathbf{u}_0|\delta\mathbf{v}_0|$, Lyapunov exponent reads

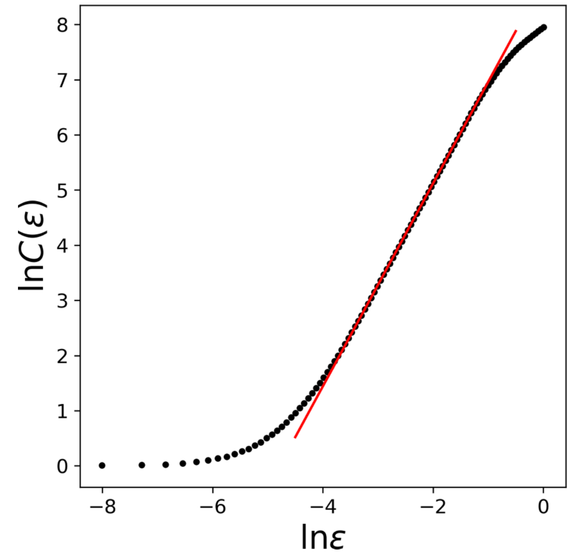

FIG. 5. The estimation of the correlation dimension for $r = 0.75$. The slope near the inflection point is best fitted with the linear dependence given by $\ln C = 8.80 + 1.84 \ln \varepsilon$.

[3,43,44]

$$\lambda(\mathbf{v}_0, \mathbf{u}_0) = \lim_{n\to\infty} \frac{1}{n} \ln \left|\mathbf{A}_{\mathbf{v}_0}^{(n)} \cdot \mathbf{u}_0\right|, \tag{18}$$

where

$$\mathbf{A}_{\mathbf{v}_0}^{(n)} = \mathbf{A}_{\mathbf{v}_{n-1}} \cdot \mathbf{A}_{\mathbf{v}_{n-2}} \cdot \ldots \cdot \mathbf{A}_{\mathbf{v}_0}, \tag{19}$$

and $\mathbf{v}_0, \mathbf{v}_1, \mathbf{v}_2, \ldots$ is the trajectory. Alternatively

$$\lambda(\mathbf{v}_0, \mathbf{u}_0) = \lim_{n\to\infty} \frac{1}{2n} \ln \left(\mathbf{u}_0^T \cdot \mathbf{H}_{\mathbf{v}_0}^{(n)} \cdot \mathbf{u}_0\right), \tag{20}$$

where

$$\mathbf{H}_{\mathbf{v}_0}^{(n)} = \left(\mathbf{A}_{\mathbf{v}_0}^{(n)}\right)^T \cdot \mathbf{A}_{\mathbf{v}_0}^{(n)}. \tag{21}$$

Numerical approximations give

$$\lambda(\mathbf{v}_0, \mathbf{u}_0) = \frac{1}{2n} \ln \left(\mathbf{u}_0^T \cdot \mathbf{H}_{\mathbf{v}_0}^{(n)} \cdot \mathbf{u}_0\right) \tag{22}$$

for large n. Choosing $\mathbf{u}_0$ along the direction of the eigenvectors of $\mathbf{H}_{\mathbf{v}_0}^{(n)}$ we obtain three Lyapunov exponents, $\lambda_1 \geqslant \lambda_2 \geqslant \lambda_3$. To evaluate them numerically we used the standard procedure of Benettin *et al.* [45], described in [3].

According to the Pesin theorem, the dynamical entropy H_{KS} of Kolmogorov and Sinai is given by the sum of positive Lyapunov exponents [44],

$$H_{KS} = \sum_{j=1}^{J} \lambda_J, \tag{23}$$

where J is the largest index such that $\lambda_j > 0$. For nonchaotic systems $H_{KS} = 0$ while chaotic system are defined by the condition $H_{KS} > 0$.

Changes of the dynamics of the system as a function of the damping parameter r is shown in Fig. 6, in which the bifurcation diagram can be compared with the Lyapunov exponents λ_i. As the second exponent λ_2 of the system analyzed

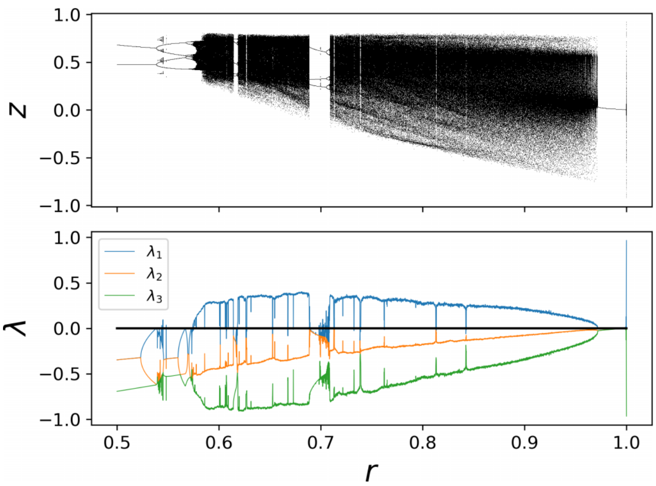

FIG. 6. Bifurcation diagram for the Z coordinate of the Bloch vector (top) to be compared with Lyapunov exponents λ_j plotted as functions of the system parameter r. The onset of chaos corresponds to positivity of the largest exponent λ_1.

is not positive, the dynamical entropy H_{KS}, equal to the sum of positive exponents, reads in this case $H_{KS} = \max\{\lambda_1, 0\}$. Observe that the entropy is positive around $r \approx 0.7$ at the right part of the three-window, in which the secondary bifurcation diagram leads to a small scale chaos. Furthermore, the system becomes (weakly) chaotic also at $r \approx 0.545$ as the secondary bifurcation scenario visible in Fig. 7 appear in parallel to the four-cycle of the main bifurcation tree.

VIII. SELF-SIMILARITY

In this section we discuss certain peculiar features of the bifurcation scheme of the map (7) corresponding to the quantum model studied in this work, which do not appear in the universal Feigenbaum bifurcation scheme, applicable to classical, one-dimensional maps with a single extremum. In such a standard scheme one observes higher order period doubling scheme which occur *inside* the windows of regular motion. For instance, the first bifurcation inside the period-3 window, corresponding to logistic map, leads to oscillations of period 6 and eventually leads to a small-scale chaotic dynamics at the right end of the window. Higher order diagrams can also be found as an entire cascade of self-affine copies of the Feigenbaum bifurcation trees can be identified—see the analysis of the magnified diagrams presented in [46].

Observe, however, that the branching pattern presented in Fig. 3 is qualitatively different, as the secondary bifurcation tree localized for $r \sim 0.5455$ appears in parallel to period-4 oscillations, before the main bifurcation scheme culminates in the onset of large scale chaotic dynamics at $r_\infty \approx 0.578$. To emphasize a self-similar structure of the investigated bifurcation scheme we present the values of the Z component of the Bloch vector in magnification of the region $r_{s_1} \approx 0.5378 < r < r_{s_2} \approx 0.5455$ shown in Fig. 7(a). It is not difficult to identify ternary bifurcation structures visualized by red rectangle at $r \sim 0.540$.

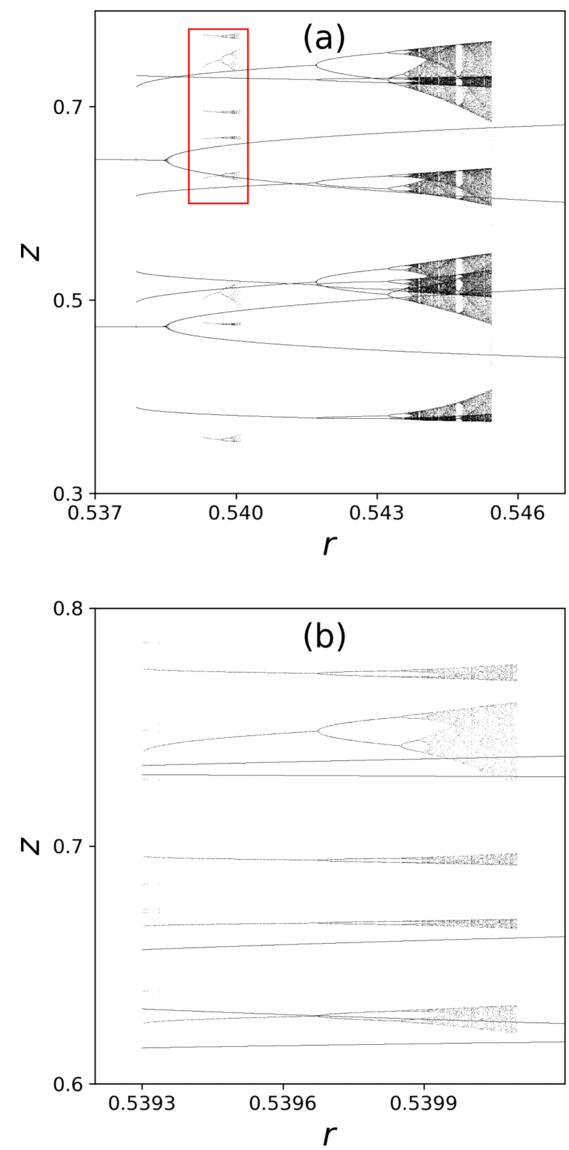

FIG. 7. Magnification of Fig. 3: (a) secondary bifurcation diagrams occurring at $r \approx 0.544$ inside the four-cycle of the main bifurcation tree; (b) magnification of the rectangle from the upper panel show a ternary structure at $r \approx 0.540$.

Similar structures, observed for the classical, two-dimensional Hénon map [34], can suggest that these effects are due to the fact that the analyzed map (7) is three dimensional. In Fig. 8 we present the behavior of the other two components of the Bloch vector in the same range of the damping parameter r. These results show that an analogous self-similar Feigenbaum structure is characteristic to all three components of the Bloch vector.

IX. CONCLUDING REMARKS

In this work we investigated the system of several interacting qubits, which realize the dynamics of the kicked top and undergo the damping described by two Kraus operators. In the case where the classical system is fully chaotic, the dynamics depends exclusively on the value of the damping parameter

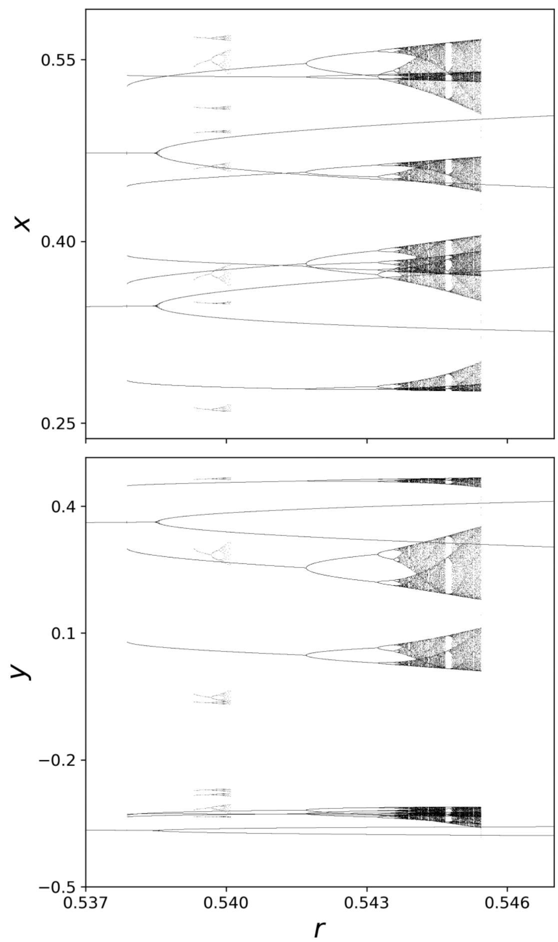

FIG. 8. Secondary bifurcation diagrams for the X and Y coordinates of the Bloch vector visible in the same parameter range, $r \approx 0.545$, as shown in Fig. 7(a).

$r \in [0, 1]$. In the case $r = 0$ the system converges to the stationary state in a single step, while for $r = 1$ (no damping) the quantum dynamics is unitary and the corresponding classical dynamics is fully chaotic. Therefore, during the parameter change we observe a transition from order to chaos. Furthermore, while decreasing the damping parameter we identify the period doubling sequence characteristic to the Feigenbaum scenario, originally discovered for one-dimensional dynamical systems.

The model of coupled spins subjected to the damping channel introduced in this work provides an example of a quantum system for which the route from regular to chaotic dynamics according to the universal scenario of Feigenbaum is reported. In contrast to the standard approach, in which the transition occurs while the nonlinearity parameter is varied [3,14], in the present study the corresponding classical dynamics is chaotic, and the period doubling takes place as the system parameter r is increased, so that the damping parameter $r' = 1 - r$ is decreased.

Interestingly, the numerical value of the ratio δ between consecutive values of the period-doubling values r_n of the damping parameter is close to the universal Feigenbaum constant derived for one-dimensional nonlinear transformations [5,6]. It is tempting to conjecture that the observed transition from regular to chaotic dynamics is not restricted to this particular model of quantum dynamics, but it correctly describes parametric changes of a wide class of many-body quantum systems.

As the system parameter r is varied one can identify cycles of oscillatory motion and windows of periodic motion ordered according to the celebrated Sharkovsky order [39–41]. However, we observe also self-similar structures analogous to the entire Feigenbaum bifurcation tree, localized in the regime of stable motion with period 4. Such a behavior, earlier reported for the two-dimensional Hénon map [34], can be related to the fact that the investigated map (7) is three dimensional.

ACKNOWLEDGMENTS

It is a pleasure to thank A. Chia for several inspiring discussions and helpful remarks. Financial support by the Foundation for Polish Science under the Team-Net Project No. POIR.04.04.00-00-17C1/18-00, the IRAP project ICTQT Contract No. 2018/MAB/5 (co-financed by EU via Smart Growth Operational Programme) and by Narodowe Centrum Nauki under Maestro Grant No. DEC-2015/18/A/ST2/00274, Maestro Grant No. DEC-2019/34/A/ST2/00081, and OPUS Grant No. DEC-2017/27/B/ST2/02959 is gratefully acknowledged.

APPENDIX

Here we show how an effective nonlinear dynamics emerges in a multiqudit system. Consider a single qudit in a state

$$\rho = \sum_{j,k=1}^{d} \rho_{j,k} |j\rangle\langle k| \tag{A1}$$

and an observable

$$A = \sum_{j=1}^{d} a_j |j\rangle\langle j|. \tag{A2}$$

Next, consider N copies of state ρ, i.e., $\rho^{\otimes N}$ and a collective observable on N qudits,

$$\mathbb{A} = \sum_{n=1}^{N} A_n, \tag{A3}$$

where

$$A_n = \mathbb{1}^{\otimes(n-1)} \otimes A \otimes \mathbb{1}^{\otimes(N-n)}. \tag{A4}$$

We are going to consider the N qudit Hamiltonian

$$H = g\mathbb{A}^2 = g \sum_{n,m=1}^{N} A_n A_m. \tag{A5}$$

This Hamiltonian is symmetric, i.e., it does not change under the permutation of qudits. Let us analyze what is the dynamics of a single qudit. The above Hamiltonian is symmetric, therefore each qudit evolves the same way, hence we can choose any qudit, say the one corresponding to $n = 1$. We can rewrite the Hamiltonian as

$$H = g\left(\sum_{n=2}^{N} A_n^2 + 2\sum_{n<m}^{N} A_n A_m\right) + g\left(A_1^2 + 2\sum_{n=2}^{N} A_1 A_n\right) = H_{\rm env} + H_1. \quad (A6)$$

The part H_1 acts on the qudit we are interested in, whereas $H_{\rm env}$ acts on the remaining qudits, which can be treated as an environment. Note that H_1 and $H_{\rm env}$ commute (in general all the terms within these Hamiltonians commute), hence the dynamics of the system is given by

$$e^{-iHt} = e^{-iH_{\rm env}t} e^{-iH_1 t}, \quad (A7)$$

where t is the time of the evolution. Therefore, the dynamics of the qudit of interest is determined by

$$e^{-iH_1 t} = e^{i(\chi/2)A_1^2} e^{i\chi A_1 A_2} e^{i\chi A_1 A_3} \dots e^{i\chi A_1 A_N} = U_1 V_2 V_3 \dots V_N, \quad (A8)$$

where $\chi = -2gt$.

Let us analyze the action of V_N on the first qudit (the one we are interested in) and the Nth qudit [remember that both are in the state ρ given by Eq. (A1)]

$$V_N(\rho\otimes\rho)V_N^\dagger = \sum_{j,k,j',k'} e^{i\chi(a_j a_{j'} - a_k a_{k'})} \rho_{j,k}\rho_{j',k'} |j\rangle\langle k| \otimes |j'\rangle\langle k'|. \quad (A9)$$

After tracing out the Nth qudit we get

$$\rho^{(1)} = {\rm Tr}_N\{V_N(\rho\otimes\rho)V_N^\dagger\} = \sum_{j,k,j'=1}^{d} p_{j'} e^{i\chi a_{j'}(a_j - a_k)} \rho_{j,k}|j\rangle\langle k| = \sum_{j,k=1}^{d} \gamma_{j,k}\rho_{j,k}|j\rangle\langle k|, \quad (A10)$$

where $p_{j'} \equiv \rho_{j',j'}$ and

$$\gamma_{j,k} = \sum_{j'=1}^{d} p_{j'} e^{i\chi a_{j'}(a_j - a_k)}. \quad (A11)$$

Next, let us consider the subsequent action of V_{N-1} on the first qudit (now in state $\rho^{(1)}$) and the $(N-1)$-th qudit (in state ρ)

$$V_{N-1}(\rho^{(1)}\otimes\rho)V_{N-1}^\dagger = \sum_{j,k,j',k'} e^{i\chi(a_j a_{j'} - a_k a_{k'})} \gamma_{j,k}\rho_{j,k}\rho_{j',k'} |j\rangle\langle k| \otimes |j'\rangle\langle k'|. \quad (A12)$$

After tracing out the $(N-1)$-th qudit we get

$$\rho^{(2)} = {\rm Tr}_{N-1}\{V_{N-1}(\rho\otimes\rho)V_{N-1}^\dagger\} = \sum_{j,k,j'=1}^{d} p_{j'} e^{i\chi a_{j'}(a_j - a_k)} \gamma_{j,k}\rho_{j,k}|j\rangle\langle k| = \sum_{j,k=1}^{d} \gamma_{j,k}^2 \rho_{j,k}|j\rangle\langle k|, \quad (A13)$$

Therefore, it is clear that after applying the sequence of operations $V_2V_3\dots V_N$ the qudit of interest is in the state

$$\rho^{(N-1)} = \sum_{j,k=1}^{d} \gamma_{j,k}^{N-1} \rho_{j,k}|j\rangle\langle k|. \quad (A14)$$

Finally, let us assume that $\chi = \frac{\theta}{N-1}$, where θ is some finite constant, and that $N\to\infty$. Note, that we define $\chi = -2gt$, which means that either the time of interaction is short, or that the interaction is weak. Here we follow the common choice made in the kicked top literature (see, e.g., [15]) and assume that the interaction scales as $1/N$. We get

$$\begin{aligned}\lim_{N\to\infty}\gamma_{j,k}^{N-1} &= \lim_{N\to\infty}\left(\sum_{j'=1}^{d} p_{j'} e^{i[\theta/(N-1)]a_{j'}(a_j-a_k)}\right)^{N-1} \\ &= \lim_{N\to\infty}\left(\sum_{j'=1}^{d} p_{j'}\left(1 + i\frac{\theta a_{j'}(a_j - a_k)}{N-1} + O(N^{-2})\right)\right)^{N-1} \\ &= \lim_{N\to\infty}\left(1 + i\frac{\theta\langle A\rangle(a_j - a_k)}{N-1} + O(N^{-2})\right)^{N-1} \\ &= e^{i\theta\langle A\rangle(a_j - a_k)}. \end{aligned} \quad (A15)$$

Therefore

$$\lim_{N\to\infty}\rho^{(N-1)} = \sum_{j,k=1}^{d} e^{i\theta\langle A\rangle(a_j-a_k)}\rho_{j,k}|j\rangle\langle k|, \quad (A16)$$

hence in the limit $N\to\infty$ the sequence of operations $V_2V_3\dots V_N$ becomes an effective single-qudit nonlinear operation

$$\lim_{N\to\infty} V_2V_3\dots V_N \equiv V_{nl} = e^{i\theta\langle A\rangle A}. \quad (A17)$$

Moreover, in the limit $N\to\infty$ we obtain

$$\lim_{N\to\infty} U_1 = \lim_{N\to\infty} e^{i\frac{\theta}{2(N-1)}A_1^2} = \mathbb{1}, \quad (A18)$$

therefore we conclude that in the limit of large N and weak interaction the dynamics of each single qudit is effectively governed by a nonlinear transformation

$$V_{nl}\rho V_{nl}^\dagger = e^{i\theta\langle A\rangle A}\rho e^{-i\theta\langle A\rangle A}. \quad (A19)$$

[1] S. H. Strogatz, *Nonlinear Dynamics and Chaos*, 2nd ed. (CRC, Boca Raton, 2018).
[2] K. T. Alligood, T. D. Sauer, and J. A. Yorke, *Chaos: An Introduction to Dynamical Systems* (Springer-Verlag, New York, 1996).
[3] E. Ott, *Chaos in Dynamical Systems*, 2nd ed. (Cambridge University Press, Cambridge, UK, 2002).
[4] H. Peitgen, H. Jürgens, and D. Saupe, *Chaos and Fractals: New Frontiers of Science* (Springer-Verlag, New York, 1992).
[5] M. Feigenbaum, Quantitative universality for a class of nonlinear transformations, J. Stat. Phys. **19**, 25 (1978).
[6] M. Feigenbaum, Universal behavior in non-linear systems, Los Alamos Sci. **1**, 4 (1980).
[7] A. Lasota and M. C. Mackey, *Chaos, Fractals and Noise* (Springer, New York, NY, 1994).
[8] M. Berry and M. Tabor, Level clustering in the regular spectrum, Proc. R. Soc. London, Ser. A **356**, 375 (1977).
[9] M. C. Gutzwiller, *Chaos in Classical and Quantum Mechanics* (Springer, New York, NY, 1990).
[10] M. Berry, Quantum chaology, not quantum chaos, Phys. Scr. **40**, 335 (1989).
[11] F. Haake, *Quantum Signatures of Chaos* (Springer-Verlag, Berlin, 1990).
[12] F. Haake, S. Gnutzman, and M. Kuś, *Quantum Signatures of Chaos*, 4th ed. (Springer-Verlag, Berlin, 2019).
[13] M. L. Mehta, *Random Matrices* (Academic, New York, 2004).
[14] P. Cvitanović, R. Artuso, R. Mainieri, G. Tanner, and G. Vattay, *ChaosBook*, on-line version at ChaosBook.org (2021).
[15] F. Haake, M. Kuś, and R. Scharf, Classical and quantum chaos for a kicked top, Z. Phys. B **65**, 381 (1987).
[16] M. Kuś, R. Scharf, and F. Haake, Symmetry versus degree of level repulsion for kicked quantum systems, Z. Phys. B **66**, 129 (1987).
[17] H.-J. Stöckmann, *Quantum Chaos: An Introduction* (Cambridge University Press, Cambridge, UK, 1999).
[18] F. Waldner, D. R. Barberis, and H. Yamazaki, Route to chaos by irregular periods: Simulations of parallel pumping in ferromagnets, Phys. Rev. A **31**, 420 (1985).
[19] S. Chaudhury, A. Smith, B. E. Anderson, S. Ghose, and P. S. Jessen, Quantum signatures of chaos in a kicked top, Nature (London) **461**, 768 (2009).
[20] V. R. Krithika, V. S. Anjusha, U. T. Bhosale, and T. S. Mahesh, NMR studies of quantum chaos in a two-qubit kicked top, Phys. Rev. E **99**, 032219 (2019).
[21] P. A. Miller and S. Sarkar, Signatures of chaos in the entanglement of two coupled quantum kicked tops, Phys. Rev. E **60**, 1542 (1999).
[22] J. N. Bandyopadhyay and A. Lakshminarayan, Entanglement production in coupled chaotic systems: Case of the kicked tops, Phys. Rev. E **69**, 016201 (2004).
[23] R. Demkowicz-Dobrzański and M. Kuś, Global entangling properties of the coupled kicked tops, Phys. Rev. E **70**, 066216 (2004).
[24] C. M. Trail, V. Madhok, and I. H. Deutsch, Entanglement and the generation of random states in the quantum chaotic dynamics of kicked coupled tops, Phys. Rev. E **78**, 046211 (2008).
[25] D. Braun, *Dissipative Quantum Chaos and Decoherence* (Springer-Verlag, Berlin, 2001).
[26] H. Fujisaki, T. Miyadera, and A. Tanaka, Dynamical aspects of quantum entanglement for weakly coupled kicked tops, Phys. Rev. E **67**, 066201 (2003).
[27] X. Wang, S. Ghose, B. C. Sanders, B. Hu, Entanglement as a signature of quantum chaos, Phys. Rev. E **70**, 016217 (2004).
[28] A. Piga, M. Lewenstein, and J. Q. Quach, Quantum chaos and entanglement in ergodic and nonergodic systems, Phys. Rev. E **99**, 032213 (2019).
[29] T. Herrmann, M. F. I. Kieler, F. Fritzsch, and A. Bäcker, Entanglement in coupled kicked tops with chaotic dynamics, Phys. Rev. E **101**, 022221 (2020).
[30] Z. Puchała, Ł. Pawela, and K. Życzkowski, Distinguishability of generic quantum states, Phys. Rev. A **93**, 062112 (2016).
[31] A. Bendersky, J. P. Paz, and M. Terra Cunha, General Theory of Measurement with Two Copies of a Quantum State, Phys. Rev. Lett. **103**, 040404 (2009).
[32] H. Bechman-Pasquinucci, B. Huttner, and N. Gisin, Nonlinear quantum state transformation of spin-1/2, Phys. Lett. A **242**, 198 (1998).
[33] L. Hardy and D. D. Song, Nonlinear qubit transformations, Phys. Rev. A **64**, 032301 (2001).
[34] Z. T. Zhusbaliyev, V. N. Rudakov, E. A. Soukhoterin, and E. Mosekilde, Bifurcation analysis of the Henon map, Discrete Dyn. Nat. Soc. **5**, 203 (2000).
[35] D. Wojcik, I. Bialynicki-Birula, and K. Życzkowski, Time Evolution of Quantum Fractals, Phys. Rev. Lett. **85**, 5022 (2000).
[36] A. Łoziński, K. Życzkowski, and W. Słomczyński, Quantum iterated function systems, Phys. Rev. E **68**, 046110 (2003).
[37] A. Jadczyk, *Quantum Fractals* (World Scientific, Singapore, 2014).
[38] M. A. Nielsen and I. L. Chuang, *Quantum Computation and Quantum Information* (Cambridge University Press, Cambridge, UK, 2010).
[39] A. N. Sharkovsky, Coexistence of cycles of continuous mapping of the line into itself, Ukrainian Math. J. **16**, 61 (1964).
[40] T.-Y. Li and J. A. Yorke, Period three implies chaos, Am. Math. Mon. **82**, 985 (1975).
[41] A. N. Sharkovsky, Universal phenomena in some infinite-dimensional dynamical systems, Int. J. Bifurcation Chaos **05**, 1419 (1995).
[42] P. Grassberger and I. Procaccia, Measuring the strangeness of strange attractors, Phys. D (Amsterdam, Neth.) **9**, 189 (1983).
[43] M. Viana, *Lectures on Lyapunov Exponents* (Cambridge University Press, Cambridge, UK, 2014).
[44] A. Pikovsky and A. Politi, *Lyapunov Exponents. A Tool to Explore Complex Dynamics* (Cambridge University Press, Cambridge, UK, 2016).
[45] G. Benettin, L. Galgani, A. Giorgilli, and J. M. Strelcyn, Lyapunov characteristic exponents for smooth dynamical systems and for hamiltonian systems; A method for computing all of them. Part 2: Numerical application, Meccanica **15**, 21 (1980).
[46] B. Luque, L. Lacasa, F. J. Ballesteros, and A. Robledo, Analytical properties of horizontal visibility graphs in the Feigenbaum scenario, Chaos **22**, 013109 (2012).